Available online at www.sciencedirect.com

SCIENCE DIRECT®

Trans. Nonferrous Met. Soc. China 18(2008) 897−903

Transactions of Nonferrous Metals Society of China

www.csu.edu.cn/ysxb/

Synthesis and characterization of Sm^{3+}-doped CeO_2 powders

LIU Guo-cong(刘国聪)[1, 2, 3], CHEN Li-miao(陈立妙)[2], DUAN Xue-chen(段学臣)[1], LIANG Da-wen(梁达文)[3]

1. School of Materials Science and Engineering, Central South University, Changsha 410083, China;
2. School of Chemistry and Chemical Engineering, Central South University, Changsha 410083, China;
3. Department of Chemistry, Yuling Normal University, Yuling 537000, China

Received 23 July 2007; accepted 5 November 2007

Abstract: Sm^{3+}-doped CeO_2 (denoted as $Ce_{1-x}Sm_xO_2$) powders with different morphologies were successfully synthesized via a precursor-growth-calcination approach, in which precursor was first synthesized by a hydrothermal method and $Ce_{1-x}Sm_xO_2$ powders were finally obtained through a calcination process. The products were characterized with X-ray diffractometry(XRD), field emission scanning electron microscopy(FE-SEM) and fluorescence spectroscopy. The results reveal that the $Ce_{1-x}Sm_xO_2$ powders obtained by calcining the precursors prepared in the absence and presence of poly(vinyl pyrrolidone) (PVP) exhibit bundle- and sphere-like morphology, respectively. The possible growth process was proposed by preparing a series of intermediate morphologies during the shape evolution of CeO_2 based on the SEM image observation. It is also found that the luminescence intensity of bundle-like $Ce_{1-x}Sm_xO_2$ is enhanced in comparison with that of sphere-like one due to its special morphology.

Key words: cerium dioxide; precursor; crystal morphology; fluorescence

---

1 Introduction

Cerium oxide(CeO_2) is a rare earth oxide that has attracted a great deal of interest owing to its unique properties, including high mechanical strength, oxygen ion conductivity and oxygen storage capacity. Because of these characteristics, CeO_2 has been widely used as an oxygen ion conductor in solid oxide fuel cells, oxygen pumps, and amperometric oxygen monitors[1−6]. CeO_2 has also been used as a gate oxide in metal oxide semiconductor devices, as a catalytic material for three-way catalysis(TWC) of exhaust gas from automobiles and fluid catalytic cracking(FCC) and as phosphor materials including both hosts and activators[7−11]. Since shape is known to be an important factor in determining the structural, physical and chemical properties of nanoparticles[12−14], there are great efforts in the shape-controlled synthesis of CeO_2 nanocrystals. CeO_2 nanoparticles and nanorods were synthesized by solution-based hydrothermal method [15−17]. Polycrystalline CeO_2 nanowires were obtained by a thermostatic bath approach using sodium bis (2-ethylhexyl) sulfosuccinate as a structure-directing agent[18]. Spindle-like CeO_2 was prepared by a polyol method[19]. CeO_2 triangular microplates were obtained from decomposition of cerium hydroxycarbonates produced by hydrothermal process[20]. However, there were no reports on the synthesis of micrometer-sized CeO_2 powders with bundle- and sphere-like morphologies.

In previous research, Eu-doped YVO_4 and Ga_2O_3 particles were synthesized with bundle-like morphology by a hydrothermal method, and it was found that the bundle-like YVO_4**:**Eu and Ga_2O_3**:**Eu particles exhibited unusual luminescence properties due to their special shape[18−19]. In this work, $Ce_{1-x}Sm_xO_2$ powders with bundle- and sphere-like morphologies are synthesized via a precursor-growth-calcination approach. The approach involves first the synthesis of cerium oxalate hydrate as the precursor by hydrothermal method and then their thermal decomposition by calcination to produce the final products. The selective fluorescence characteristics of $Ce_{1-x}Sm_xO_2$ are also studied.

Foundation item: Project(20676153) supported by the Science Foundation of Guangxi Provincial Education Department, China; Project(0728107) supported by the Science and Technology Bureau of Guangxi Province, China; Project(08JJ3104) supported by the Natural Science Foundation of Hunan Province, China

Corresponding author: LIU Guo-cong; Tel: +86-731-8830503; E-mail: gcl_109@163.com

2 Experimental

2.1 Preparation of precursor and products

All reagents were analytically pure and used without further purification. The hydrothermal reactions were carried out in a stainless steel autoclave with a Teflon liner (100 mL in total capacity) under autogenous pressure. In a typical synthesis, 4 mmol nitrate (including 3.92 mmol $Ce(NO_3)_3{\cdot}6H_2O$ and 0.08 mmol $Sm(NO_3)_3{\cdot}6H_2O$) and 6 mmol $Na_2C_2O_4$ were, respectively, dissolved in 30 mL deionized water to obtain aqueous solutions. After predetermined amount of PVP aqueous solution (0.2 mol/L in repeating unit, 1 300 000 in average relative molecular mass, Acros Organics) was introduced into the $Ce(NO_3)_3{\cdot}6H_2O$ solution, the two solutions were thoroughly mixed by vigorous stirring. The resulting suspension was successively put into an autoclave, and the autoclave was filled with deionized water up to 80% of the total volume. Hydrothermal synthesis was carried out at 180 ℃ for 8 h. After cooling to room temperature naturally, the white precipitate was collected, washed with distilled water and absolute ethanol several times, and then dried in air at 60 ℃ for 4 h. Subsequently, the as-synthesized precursors were calcined in air at 800 ℃ for 4 h to produce $Ce_{1-x}Sm_xO_2$ powders.

2.2 Analysis of products

All the samples were characterized by X-ray powder diffraction(XRD) using a Bruker D8-advance X-ray diffractometer with Cu K_α radiation (λ=1.541 8 Å). XRD patterns were recorded from 10° to 70° (2θ) with a scanning step of 0.01°. The size distribution and morphology of the samples were analyzed by field emission scanning electron microscopy(FE-SEM, Sirion200, FEI, GENESIS 60S, American). The excitation and emission spectra were measured with a Hitachi F-2500 fluorescence spectrometer.

3 Results and discussion

3.1 XRD analysis

Figs.1(a) and (b) show the XRD patterns of the precursors prepared in the absence and presence of PVP, respectively. It is found that all the samples are composed of cerium oxalate hydrate (JCPDS card 14-0710) and some unidentified phase. The width of the diffraction peaks for the sample prepared in the absence of PVP indicates high crystallinity and large particle size. Figs.1(c) and (d) show the typical XRD patterns of the products obtained by calcining the precursor at 800 ℃ for 4 h. All the peaks can be indexed as fluorite-structured CeO_2 phase (JCPDS card 19-0284). The comparison of the patterns shows that the CeO_2:Sm^{3+} obtained by pyrolyzing the precursor prepared in the presence of PVP has wide diffraction peaks, indicating small particle size.

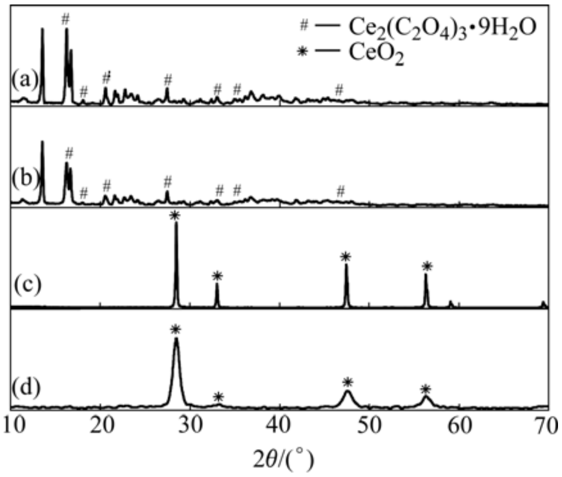

Fig.1 XRD patterns of precursors prepared in absence of PVP (a) and in presence of PVP (b); CeO_2:Sm^{3+} products obtained by calcining precursor prepared in absence of PVP (c) and in presence of PVP (d)

3.2 SEM analysis

The morphologies and microstructure of the precursors and $Ce_{1-x}Sm_xO_2$ products were investigated using SEM. It is found that the $Ce_{1-x}Sm_xO_2$ products retain the morphology of the precursors exactly. Here only SEM images of the $Ce_{1-x}Sm_xO_2$ products are presented. Fig.2(a) shows the typical image of the $Ce_{1-x}Sm_xO_2$ products obtained by calcining the precursors, which was synthesized from the solutions without PVP after hydrothermal heat-treatment at 180 ℃ for 8 h. The SEM image indicates that a large amount of micrometer-sized bundles (with length up to about 60 μm) appear as sheaves of straw tied in the middle, forming the straw-tied-like microstructure of $Ce_{1-x}Sm_xO_2$. Fig.2(b) presents the typical image of individual straw-tied-like bundle. A careful observation of the image reveals that $Ce_{1-x}Sm_xO_2$ bundle is composed of microrods with inhomogeneous size distribution of diameter. Fig.2(c) shows the SEM image of the tied region at high magnification. It is clear that the rods grow across each other to form straw-tied-like structures. In addition to the bundle-like morphology, half-bundle-like (Fig.2(d)) and rod-like (not shown here) morphologies are also observed in the samples. The majority of $Ce_{1-x}Sm_xO_2$ structures is bundle, and the minority is half-bundle and rod.

Several time-dependent experiments were carried

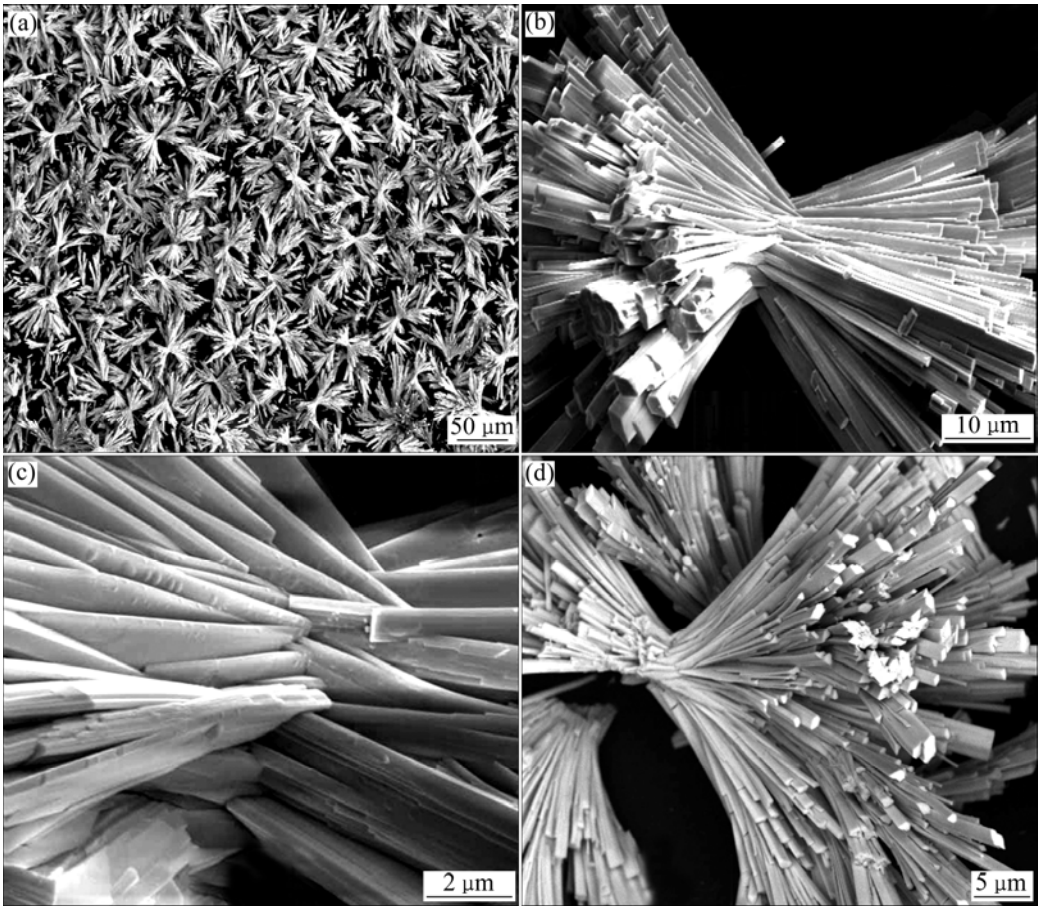

Fig.2 SEM images of $Ce_{1-x}Sm_xO_2$ obtained by calcining precursors synthesized from solutions after hydrothermal heat-treatment at 180 ℃ for 8 h: (a) $Ce_{1-x}Sm_xO_2$ products; (b) Individual straw-tied-like bundle; (c) High-magnification image of tied region; (d) Half-bundle-like morphology

out by quenching the Teflon-lined autoclave with cold water at different reaction stages to investigate the growth mechanism of bundle-like $Ce_{1-x}Sm_xO_2$. The precursors obtained from the solution after hydrothermal heat-treatment at 180 ℃ for 0, 2, 4 and 8 h are denoted as S_1, S_2, S_3 and S_4, respectively. Figs.3(a)−(f) show the SEM images of the $Ce_{1-x}Sm_xO_2$ products obtained by calcining S_1, S_2, S_3 and S_4, respectively. These images exhibit the evolution of $Ce_{1-x}Sm_xO_2$ microstructures from rod to bundle. Fig.3(a) show the image of the product obtained by calcining S_1. It is clear that as-prepared product is rod-like particles with inhomogeneous size distribution, which is in agreement with literature report[20]. Fig.3(b) exhibits the image of the product obtained by calcining S_2. A large number of bundles with a length of about 7 μm and an aspect ratio of about 1.5 are observed in the product. The size and morphology of each product are comparatively uniform.

Fig.3(c) shows the typical image of individual bundle. It clearly reveals that the bundle is composed of many rods. Fig.3(d) shows the image of the product obtained by calcining S_3. It can be observed that the product takes on dumbbell-like bundle morphology, and the length (about 30 μm) and aspect ratio (about 4) increase greatly compared with those of the product obtained by calcining S_2. Fig.3(e) presents the typical image of individual dumbbell-like bundle. Careful observation reveals that two ends of the bundle grow to loose bundle. Fig.3(f) shows the image of the product obtained by calcining S_4. When prolonging the hydrothermal reaction time to 8 h, the product mainly exhibits straw-tied-like bundle morphology.

Based on above SEM observation, a possible growth process demonstrating the synthesis of precursor with straw-tied-like bundle morphology can be simply described in Fig.4. First, new born clusters of precursor agglomerate together to form rod-like particles at room temperature. And then, the rod-like particles agglomerate together to form cylindrical bundles, and the growth fronts may radiate in opposite directions and lead to the formation of the straw-tied-like bundles.

The effect of PVP on the formation of $Ce_{1-x}Sm_xO_2$ crystals with different morphologies is illustrated in Fig.5. Fig.5(a) shows the representative SEM image of

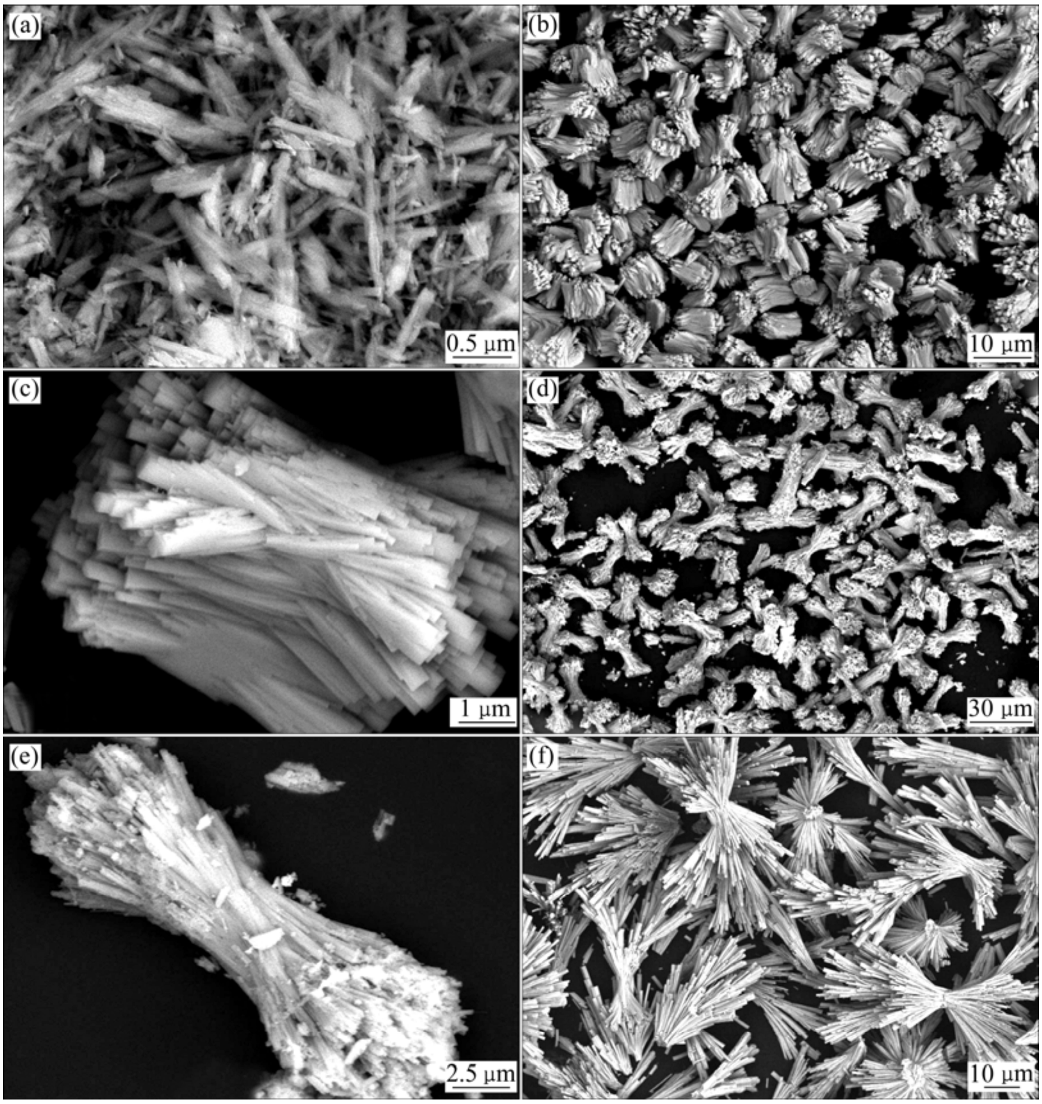

Fig.3 SEM images of $Ce_{1-x}Sm_xO_2$ product obtained by calcining precursors synthesized from solutions after hydrothermal heat-treatment at 180 ℃ for 0 h (a); 2 h (b, c); 4 h (d, e) and 8 h (f)

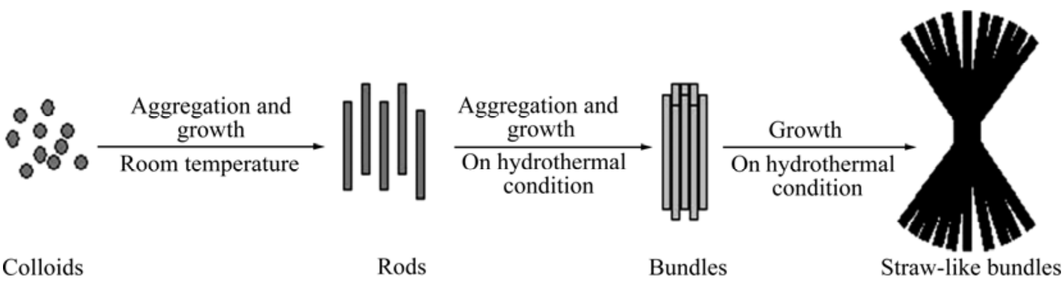

Fig.4 Schematic depicting possible growth routes for bundle-like precursors

the $Ce_{1-x}Sm_xO_2$ products obtained by using 5 mL PVP. The as-synthesized products mainly consist of micrometer-sized (about 60 μm in length) bundles and nanosized (about 100 nm in diameter) particles. Fig.5(b) shows the SEM image of the nanosized particles at high magnification. It is found that nanosized particles exhibit sphere-like morphology. When the amount of PVP is increased to 12 mL, the morphology changes greatly in comparison with that of the products shown in Fig.5(a). The as-synthesized products are mainly composed of sphere-like particles with diameter of about 100 nm. Moreover, most of the sphere-like particles agglomerate together to form string-like particles, as shown in Fig.5(c). Fig.5(d) shows the SEM image of the string-

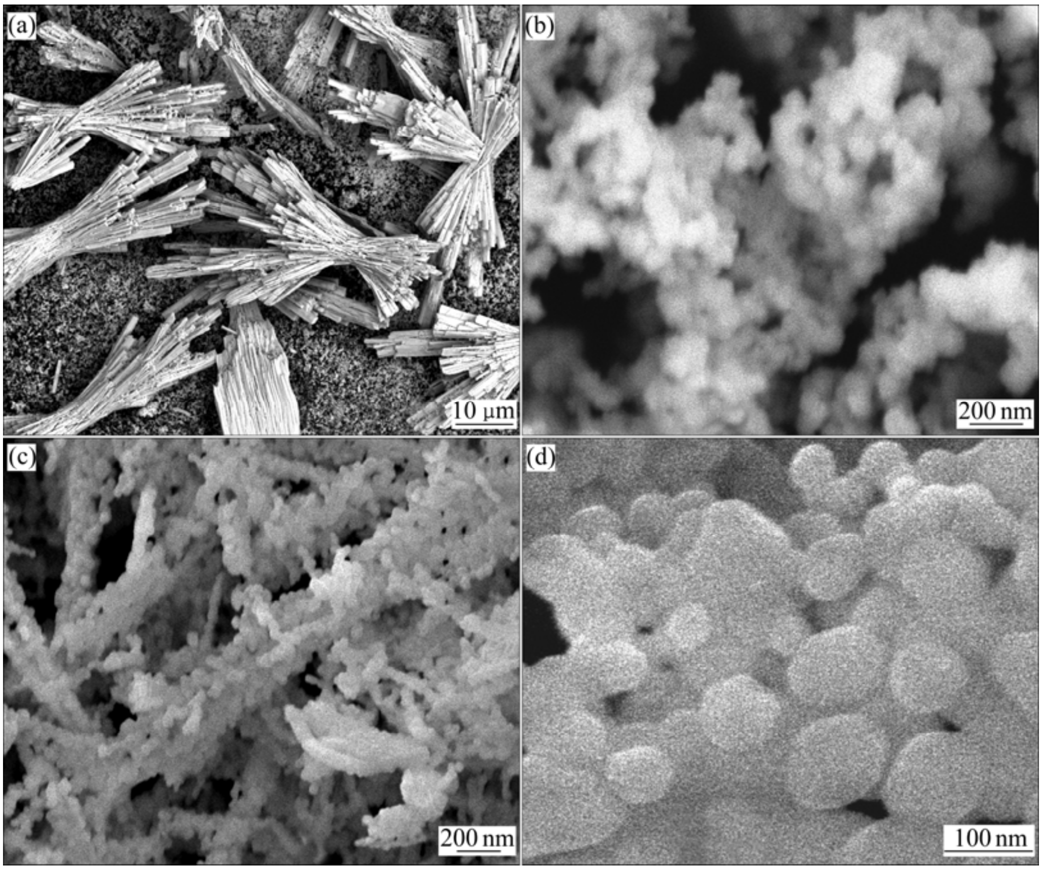

Fig.5 SEM images of $Ce_{1-x}Sm_xO_2$ products obtained by calcining precursors synthesized from solutions with 5 mL PVP (a, b) and 12 mL PVP (c, d) after hydrothermal heat-treatment at 180 ℃ for 8 h

like particles at high magnification. Above SEM observations reveal that PVP can affect the morphology and the size of final products. The relatively high amount of PVP may cause high coverage of PVP on all faces of newborn clusters of precursors, leading to an isotropic growth mode and small particle size[21].

The energy-dispersive spectrum analysis was used to analyze the composition of the bundle- and sphere-like $Ce_{1-x}Sm_xO_2$ powders. It is found that the actual mole fraction of samarium in bundle- and sphere-like $Ce_{1-x}Sm_xO_2$ powders are 1.78% and 1.83%, respectively.

3.3 Fluorescence properties

The excitation spectra monitored at the emission wavelength of 574 nm with similar shape for Sm^{3+}-doped bundle- and sphere-like $Ce_{1-x}Sm_xO_2$ particles are illustrated in Fig.6. The spectra exhibit two broad excitation bands, one band around 325−430 nm corresponding to the charge transfer between the O^{2-} valence band and the Ce^{4+} conduction band, and the other band around 260−290 nm corresponding to the charge transfer between O^{2-} and Sm^{3+}[22]. The room temperature emission spectra of bundle- and sphere-like $Ce_{1-x}Sm_xO_2$ particles under 369 nm excitation are given in Fig.7. Several apparent emission bands with a predominant peak at 574 nm are observed in each spectrum and can be distributed into two groups corresponding to different transition. The emission peaks centered at 562 and 574 nm correspond to the transition $^4G_{5/2}\rightarrow{}^6H_{5/2}$. The emission peaks centered at 593, 611, 617, and 623 nm correspond to the transition $^4G_{5/2}\rightarrow{}^6H_{7/2}$. The point-group symmetry of Ce sites in the fluorite CeO_2 structure is O_h with eight-fold oxygen coordination, thereby providing an inversion symmetry. When Sm^{3+} incorporates in CeO_2 crystals, it has the same point-group symmetry as Ce^{4+}. According to the selection rule, magnetic-dipole transitions that obey $\Delta J=0$ and ±1 (J: the total angular momentum) are allowed for Sm^{3+} in a site with inversion symmetry. Therefore, the $^4G_{5/2}\rightarrow{}^6H_{5/2}$ ($\Delta J=0$) and the $^4G_{5/2}\rightarrow{}^6H_{7/2}$ ($\Delta J=1$) transitions can be observed; while the $^4G_{5/2}\rightarrow{}^6H_{9/2}$ ($\Delta J=2$) transitions, which are usually observed in other host materials such as ZrO_2 and Y_2O_3[23−24], are strictly forbidden in $Ce_{1-x}Sm_xO_2$. Of the two samples, the emission spectra of these samples are similar in shape, and the bands differ only in their relative intensities. The emission intensity of bundle-like $Ce_{1-x}Sm_xO_2$ is higher than that of sphere-like $Ce_{1-x}Sm_xO_2$. It is well known that

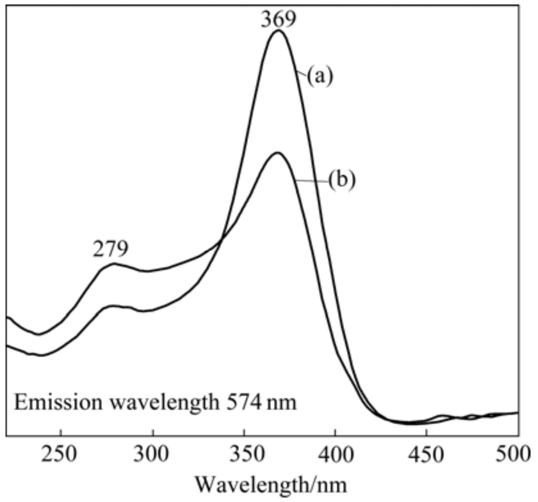

Fig.6 Excitation spectra of $Ce_{1-x}Sm_xO_2$ products: (a) With bundle-like morphology; (b) With sphere-like morphology

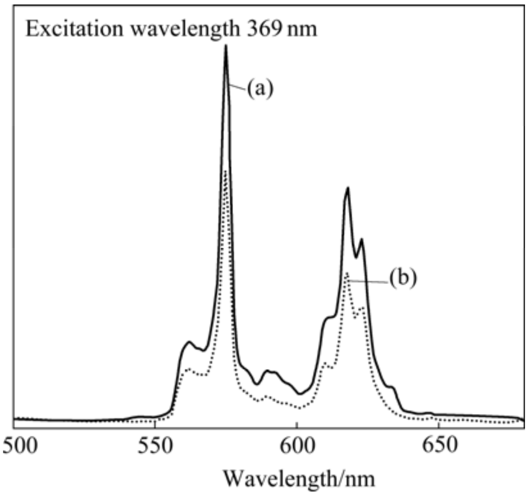

Fig.7 Emission spectra of $Ce_{1-x}Sm_xO_2$ products: (a) With bundle-like morphology; (b) With sphere-like morphology

the phosphors obtained from different routes usually have different crystallizations, which may give rise to different luminescence behavior. In our cases, the samples calcined at 800 ℃ have the same degree of crystallizations (as shown in Fig.1). So the difference of luminescence intensity should be caused by other factors. Some authors reported that the shape anisotropy could affect site symmetry of Re^{3+}, giving the different luminescence behavior[25−27]. Although much work remains to be done to fully understand the difference of intensity for bundle- and sphere-like $Ce_{1-x}Sm_xO_2$, it is speculated that the enhanced luminescence intensity of the bundle- and sphere-like $Ce_{1-x}Sm_xO_2$ is caused by its special morphology.

4 Conclusions

1) $Ce_{1-x}Sm_xO_2$ powders are synthesized by a precursor-growth-calcination approach, and it is found that $Ce_{1-x}Sm_xO_2$ powders obtained by calcining the precursors prepared in the absence and presence of PVP exhibit bundle- and sphere-like morphology, respectively.

2) The growth process of the $Ce_{1-x}Sm_xO_2$ powders with straw-tied-like bundle morphology is as follows. The newborn clusters of precursor agglomerate together to form rod-like particles at room temperature, then the rod-like particles agglomerate together to fabricate cylindrical bundles, and the growth fronts may radiate in opposite directions, leading to the formation of the straw-tied-like boundless in the hydrothermal condition.

3) The luminescence intensity of bundle-like $Ce_{1-x}Sm_xO_2$ is enhanced in comparison with that of sphere-like $Ce_{1-x}Sm_xO_2$ due to its special morphology.

References

[1] KANG Z C, WANG Z L, LI M W. Novel oxides for cycled hydrogen production from methane and water using a temperature swing [J]. Adv Mater, 2003, 15(6): 521−526.

[2] PARK S D, VOHS J M, GORTE R J. Direct oxidation of hydrocarbons in a solid-oxide fuel cell [J]. Nature, 2000, 404(6775): 265−267.

[3] PANZERA G, MODAFFERI V, CANDAMANO S, DONATO A. CO selective oxidation on ceria-supported Au catalysts for fuel cell application [J]. Power Sources, 2004, 135(1): 177−179.

[4] STEELE B C H, LIETENBURG C, BOARO M. Appraisal of $Ce_{1-y}Gd_yO_{2-y/2}$ electrolytes for IT-SOFC operation at 500 ℃ [J]. Solid State Ionics, 2000, 129(1): 95−110.

[5] TADOKORO S, PORFIRIO T, MUCCILLO R, MUCCILLO E. Synthesis, sintering and impedance spectroscopy of 8 mol% yttria-doped ceria solid electrolyte [J]. Journal of Power Sources, 2004, 130(1): 15−21.

[6] IZU N, SHIN W, MURAYARNA N, KANZAKI S. Resistive oxygen gas sensors based on CeO_2 fine powder prepared using mist pyrolysis [J]. Sensor Actuat B, 2002, 87(1): 95−98.

[7] ZHOU K, WANG X, SUN X. Enhanced catalytic activity of ceria nanorods from well-defined reactive crystal planes [J]. Journal of Catalysis, 2005, 229(1): 206−212.

[8] VALENZUELA R, BUENO G., CORBERÁN V, YU Y D, CHEN C L. Selective oxide hydrogenation of ethane with CO_2 over CeO_2-based catalysts [J]. Catalysis Today, 2000, 61(1): 43−48.

[9] VILA L D, STUCCHI E B, DAVOLOS M R. Preparation and characterization of uniform, spherical particles of Y_2O_2S and Y_2O_2S:Eu [J]. Journal of Material Chemistry, 1997, 7(10): 2113−2117.

[10] OIKAWA M, FUJIHARA S. Crystal growth of $Ce_2O(CO_3)_2{\cdot}H_2O$ in aqueous solutions: Film formation and samarium doping [J]. Journal of Solid State Chemistry, 2005, 178(6): 2036−2041.

[11] SUN C W, LI H, ZHANG H R, WANG Z. Controlled synthesis of CeO_2 nanorods by a solvothermal method [J]. Nanotechnology, 2005, 16(9): 1454−1463.

[12] ALIVISATOS A P. Semiconductor clusters, nanocrystals, and quantum dots [J]. Science, 1996, 271: 933−937.

[13] HUIGNARD A, GACOIN T, BOILOT J P. Synthesis and luminescence properties of colloidal YVO_4:Eu phosphors [J].

Chemistry of Materials, 2000, 12(4): 1090−1094.

[14] CHEN L M, LIU Y N, LU Z G, ZENG D M. Shape-controlled synthesis and characterization of $InVO_4$ particles [J]. Journal of Colloid and Interface Science, 2006, 295: 440−444.

[15] HO C M, YU J, KWONG T. Morphology-controllable synthesis of mesoporous CeO_2 nano- and microstructures [J]. Chemistry of Material, 2005, 17(17): 4514−4522.

[16] XU H R, GAO L, GU H C. Synthesis of solid, spherical CeO_2 particles prepared by the spray hydrolysis reaction method [J]. Journal of the American Ceramic Society, 2002, 85(1): 139−144.

[17] BOLIS V, MAGNACCA G, CERRATO G, MORTERRA C. Microcalorimetric and IR-spectroscopic study of the room temperature adsorption of CO_2 on pure and sulphated t-ZrO_2 [J]. Thermochimica Acta, 2001, 379(1): 147−61.

[18] CHEN L M, LIU Y N, HUANG K L. Hydrothermal synthesis and characterization of YVO_4-based phosphors doped with Eu^{3+} ion [J]. Materials Research Bulletin, 2006, 41(1): 158−166.

[19] XIE H B, CHEN L M, LIU Y N, HUANG K L. Preparation and photoluminescence properties of Eu-doped α- and β-Ga_2O_3 phosphors [J]. Solid State Communications, 2007, 141: 12−16.

[20] HYUN J, KIM J, KIM S, KIM D, YOON S, LEE J Y. Ultrasonic study on conglomeration of cerium oxalate particles produced by reaction crystallization in series reactor including T-mixer and stirred tank [J]. Journal of Chemical Engineer of Japan, 2002, 35(11): 1211−1218.

[21] SUN Y G, YINY D, MAYERS B T, HERRICKS T, XIA Y N. Uniform silver nanowires synthesis by reducing $AgNO_3$ with ethylene glycol in the presence of seeds and poly(Vinyl Pyrrolidone) [J]. Chemistry of Materials, 2002, 14(11): 4736−4745.

[22] FUJIHARA S, OIKAWA M, FUJIHARA S, MASA S. Structure and luminescent properties of CeO_2: rare earth (RE=Eu^{3+} and Sm^{3+}) thin films [J]. Journal of Applied Physics, 2002, 95(12): 8002−8006.

[23] DE LA ROSA-CRUZ E, DIAZ-TORRES L A, SALAS P, RODRIGUEZ A, KUMAR A. Luminescent properties and energy transfer in ZrO_2: Sm^{3+} nanocrystals [J]. Journal of Applied Physics, 2004, 94(5): 3509− 3515.

[24] ZHOU Y H, LIN J, WANG S B. Energy transfer and upconversion luminescence properties of Y_2O_3:Sm and Ga_2O_3:Sm phosphors [J]. Journal of Solid State Chemistry, 2003, 171(1/2): 391−395.

[25] WU C F, QIN W P, ZHAO G S, ZHANG J S, HUANG S H, LU S Z, LIU H Q, LIN H Y. Photoluminescence from Y_2O_3:Eu nanotubes [J]. Applied Physics Letters, 2003, 82(4): 520− 522.

[26] YU L X, SONG H W, LU S Z, LIU Z X, YANG L M. Influence of shape anisotropy on photoluminescence characteristic in $LaPO_4$:Eu nanowires [J]. Chemical Physics Letters, 2004, 399(3/6): 384−388.

[27] CHEN L M. Hydrothermal synthesis and ethanol sensing properties of $CeVO_4$ and $CeVO_4$-CeO_2 powders [J]. Materials Letters, 2006, 60: 1859−1862.

(Edited by YUAN Sai-qian)